


## Density distributions of tune shifts from space charge or beam-beam interactions in Gaussian bunches

Tanaji Sen<sup>\*</sup>*Fermi National Accelerator Laboratory, Batavia, Illinois 60510, USA* (Received 17 June 2023; accepted 14 August 2023; published 25 August 2023)

The amplitude dependent tune shifts from either space charge or beam-beam interactions are calculated analytically with the inclusion of synchrotron oscillations and multiple interactions around the ring. Simpler formulas are derived under limits of bunches longer than the transverse sizes, equal and unequal transverse sizes, etc. This is used to derive semianalytical forms for the density distribution of the tune shifts. The tune spread and the density distribution are needed to understand beam decoherence or Landau damping with either interaction. The tune footprints due to space charge in IOTA are simulated using `PyOrbit` and found to be in good agreement with the theoretical predictions.

DOI: [10.1103/PhysRevAccelBeams.26.080101](https://doi.org/10.1103/PhysRevAccelBeams.26.080101)

### I. INTRODUCTION

The space charge interaction in a low energy synchrotron and the beam-beam interaction in a collider are the dominant contributors to the incoherent tune spread in these machines. In this report, we calculate first the incoherent amplitude dependent transverse tune shifts in Gaussian beams due to either interaction. We generalize these tune shifts to include the effects of synchrotron oscillations and especially in the case of space charge, we also include the contributions of the interactions from multiple locations around the ring. Next, we calculate the beam density distributions as a function of these tuneshifts. This density distribution is needed to determine beam stability in different conditions. In terms of scaled tune shifts (defined in Sec. III), the density distribution has exactly the same form for both space charge and beam-beam interactions. However, the role of the tune spread and the density in determining beam stability is very different in the two interactions. The head-on beam-beam interactions act as an external source of tune spread and can consequently be used to provide Landau damping [1] while with space charge, an external driving source such as octupoles [2] or perhaps electron lenses [3] is required for Landau damping. Nevertheless, even with space charge, the contributions from the internal tune spread and the density distribution have to be included in determining beam stability. Another use of the incoherent tune spread with

either interaction is finding the beam decoherence time when the centroid is offset from the center, e.g., due to a dipole kick.

The calculation of tune shifts due to head-on beam-beam interactions was reported in [4–6] while the fully 2D calculation of tune spreads and resonance driving terms, etc., was done, e.g., in [7]. These were then generalized to long-range interactions [8] which were of greater interest in the Tevatron. The expressions for head-on interactions are easily found by taking the limit of zero separation. We note that the space charge tune shifts with amplitude for round beams without synchrotron oscillations were calculated in [9] which used some of the methods in [7]. The density distribution was extracted from numerical simulations, but an insufficient sampling of the beam core led to an incorrect form of the density, especially close to the core where the space charge tune shift is largest. Our method is semi-analytical, in that numerical inversion of analytical functions followed by interpolation to obtain smooth functions is required. We also check that the zeroth to second moments of the distribution are preserved.

### II. INCOHERENT TUNE SHIFTS WITH SYNCHROTRON OSCILLATIONS

Here we consider the tune shifts with amplitude due to a Hamiltonian with linear transverse motion, longitudinal motion in an rf bucket, and either a space charge interaction or a beam-beam interaction. In this section, we consider first the Hamiltonian with a space charge interaction experienced by a Gaussian distribution in three space dimensions. At the end of this section, we consider the beam-beam interaction and show that the tune shift with amplitude scaled by the zero amplitude tune shift has the same form as with space charge. The Hamiltonian in the lab frame can be written in dimensionless form as

\*tsen@fnal.gov

Published by the American Physical Society under the terms of the *Creative Commons Attribution 4.0 International license*. Further distribution of this work must maintain attribution to the author(s) and the published article's title, journal citation, and DOI.

$$H = \frac{1}{2}[(x')^2 + (y')^2 + K_x x^2 + K_y y^2] + \frac{e}{\beta^2 \gamma m_0 c^2} (V_{\text{rf}} + V_{\text{SC}}), \quad (2.1)$$

where  $(x, y, x', y')$  are the phase space coordinates,  $(K_x, K_y)$  are quadrupole strengths,  $e$  is the unit of particle charge,  $c$  is the speed of light,  $V_{\text{rf}}$  is the rf cavity voltage wave form, and  $V_{\text{SC}}$  is the electric potential due to the space charge measured in the lab frame. Transforming to action-angle variables  $(J_x, \phi_x, J_y, \phi_y)$  in the transverse planes, as, e.g.,

$$x = \sqrt{2\beta_x J_x} \cos \phi_x, \\ x' = \sqrt{2J_x} \left[ \sqrt{\frac{1}{\beta_x}} \sin \phi_x - 2\alpha_x \cos \phi_x \right]. \quad (2.2)$$

$$V(x, y, z) = \frac{1}{4\pi\epsilon_0} \frac{Ne}{\pi^{1/2}\gamma} \int_0^\infty dq \frac{1}{\sqrt{(2\sigma_x^2 + q)(2\sigma_y^2 + q)(2\gamma^2\sigma_z^2 + q)}} \left[ 1 - \exp \left[ \left( -\frac{x^2}{2\sigma_x^2 + q} - \frac{y^2}{2\sigma_y^2 + q} - \frac{\gamma^2 z^2}{2\gamma^2\sigma_z^2 + q} \right) \right] \right], \quad (2.5)$$

where the coordinates  $(x, y, z)$  and the rms sizes  $(\sigma_x, \sigma_y, \sigma_z)$  are measured in the rest frame. The complete Hamiltonian in three degrees of freedom (3 d.o.f.) after scaling by  $R$  is

$$H = \nu_{x,0} J_x + \nu_{y,0} J_y + \frac{eR}{\beta^2 \gamma m_0 c^2} V_{\text{rf}}(\delta p/p, z) + RC_{\text{SC}} \bar{V}(x, y, z), \quad (2.6)$$

$$C_{\text{SC}} = \frac{N_p r_p}{\pi^{1/2} \beta^2 \gamma^2}, \quad (2.7)$$

$$\bar{V}(x, y, z) = \int_0^\infty dq \frac{1}{\sqrt{(2\sigma_x^2 + q)(2\sigma_y^2 + q)(2\gamma^2\sigma_z^2 + q)}} \left[ 1 - \exp \left( -\frac{x^2}{2\sigma_x^2 + q} - \frac{y^2}{2\sigma_y^2 + q} - \frac{\gamma^2 z^2}{2\gamma^2\sigma_z^2 + q} \right) \right], \quad (2.8)$$

where  $r_p = e^2/(4\pi\epsilon_0 m_0 c^2)$  is the classical particle radius. The tunes follow from the derivatives of the angle-averaged Hamiltonian. We will write only the expressions in  $x$ , the one for  $y$  can be found by the replacement  $x \leftrightarrow y$ . Our focus is on the transverse tune shifts with amplitude, thus we ignore dominantly longitudinal effects such as longitudinal space charge effects. We also do not consider the momentum dependence of the transverse tunes or the modulation of the revolution period by the synchrotron oscillations, these do not have a noticeable effect on the dynamics in IOTA because of the small synchrotron tune. We do include the impact of

This reduces the linear part of the transverse Hamiltonian to

$$H_{\perp,0} = \frac{1}{R} (\nu_{x,0} J_x + \nu_{y,0} J_y), \quad (2.3)$$

where  $(\nu_{x,0}, \nu_{y,0})$  are the tunes of the linear lattice and  $R$  is the machine radius.

Consider a Gaussian distribution in three space dimensions for a bunch; the same bunch experiencing its space charge field or the opposing bunch for the case of beam-beam interactions

$$\psi(x, y, z) = \frac{Ne}{(2\pi)^{3/2} \sigma_x \sigma_y \sigma_z} \exp \left[ -\frac{x^2}{2\sigma_x^2} - \frac{y^2}{2\sigma_y^2} - \frac{z^2}{2\sigma_z^2} \right], \quad (2.4)$$

where  $\sigma_x, \sigma_y,$  and  $\sigma_z$  are the rms bunch dimensions. The solution of Poisson's equation  $\nabla^2 V = -\psi/\epsilon_0$  leads to the following solution for the electric scalar potential [10]:

synchrotron oscillations on the transverse dynamics via the nonlinear interaction potential. With these assumptions, the transverse tune shifts are given by

$$\Delta\nu_x = RC_{\text{SC}} \frac{\partial}{\partial J_x} \langle \bar{V} \rangle_{\phi_x, \phi_y, \phi_z, s}, \quad (2.9)$$

where the averaging is done over all three angles and over  $s$ , the length along the ring. Hence after using action-angle variables,

$$\Delta\nu_x = RC_{\text{SC}} \int_0^\infty dq \frac{1}{\sqrt{(2\sigma_x^2 + q)^3 (2\sigma_y^2 + q) (2\gamma^2\sigma_z^2 + q)}} 2\beta_x \cos^2 \phi_x \exp \left[ -\frac{2\beta_x J_x \cos^2 \phi_x}{2\sigma_x^2 + q} - \frac{y^2}{2\sigma_y^2 + q} - \frac{\gamma^2 z^2}{2\gamma^2\sigma_z^2 + q} \right].$$

Changing the integration variable from  $q$  to a dimensionless variable  $u$  as

$$u = \frac{2\sigma_x^2}{(2\sigma_x^2 + q)}, \Rightarrow q = \frac{2\sigma_x^2}{u} - 2\sigma_x^2.$$

This converts the infinite range of integration over  $q$  to a finite range of integration over  $u$ . Hence

$$\begin{aligned} \Delta\nu_x = & \frac{RC_{SC}\beta_x}{2^{1/2}\sigma_x^2\gamma\sigma_z} \int_0^1 du \left\langle \cos^2\phi_x \left[ \frac{1}{[(\sigma_y^2/\sigma_x^2 - 1)u + 1]} \frac{u}{[(1 - \sigma_x^2/\gamma^2\sigma_z^2)u + \sigma_x^2/\gamma^2\sigma_z^2]} \right]^{1/2} \right. \\ & \times \exp \left[ -\frac{2\beta_x J_x \cos^2\phi_x}{2\sigma_x^2} u - \frac{2\beta_y J_y \cos^2\phi_y}{2\sigma_y^2} \frac{u}{2\sigma_y^2[(1 - \sigma_x^2/\sigma_y^2)u + \sigma_x^2/\sigma_y^2]} - \frac{\gamma^2 z^2 u}{2\gamma^2\sigma_z^2[(1 - \sigma_x^2/\gamma^2\sigma_z^2)u + \sigma_x^2/\gamma^2\sigma_z^2]} \right] \left. \right\rangle_{\phi_x, \phi_y, s}. \end{aligned} \quad (2.10)$$

In order to make progress, we need to assume that the longitudinal motion is simple harmonic. This implies that the rf cavity force be linear or equivalently that we approximate the cosine term in  $V_{rf}$  by the first two terms in its Taylor expansion. Writing the coordinates  $(x, y, z)$  in terms of dimensionless amplitudes  $(a_x, a_y, a_z)$  and the corresponding rms sizes  $(\sigma_x, \sigma_y, \sigma_z)$ ,

$$x = a_x \sigma_x \cos \phi_x, \quad y = a_y \sigma_y \cos \phi_y, \quad z = a_z \sigma_z \cos \phi_z. \quad (2.11)$$

We use the integral representation of  $I_0$

$$I_0(w) = \frac{1}{\pi} \int_0^\pi d\theta \exp[\pm w \cos \theta] = \frac{1}{2\pi} \int_0^{2\pi} d\theta \exp[\pm w \cos 2\theta]. \quad (2.12)$$

The integrals in the phase averages over  $\phi_x, \phi_y, \phi_z$  are of the form

$$\frac{1}{2\pi} \int_0^{2\pi} d\phi \exp[-w \cos^2 \phi] = \exp\left[-\frac{1}{2}w\right] I_0\left(\frac{1}{2}w\right) \frac{1}{2\pi} \int_0^{2\pi} d\phi \cos^2 \phi \exp[-w \cos^2 \phi] = \frac{1}{2} \exp\left[-\frac{1}{2}w\right] \left[ I_0\left(\frac{1}{2}w\right) - I_1\left(\frac{1}{2}w\right) \right].$$

Gathering all terms together, the final expression is

$$\begin{aligned} \Delta\nu_x(a_x, a_y, a_z) = & C_{SC} \frac{R}{2\sqrt{2}\gamma\sigma_z\epsilon_x} \int_0^1 du \exp\left[-\frac{a_x^2 u}{4}\right] \left[ I_0\left(\frac{a_x^2 u}{4}\right) - I_1\left(\frac{a_x^2 u}{4}\right) \right] \exp\left[-\frac{a_y^2 u}{4}\right] \exp\left[-\frac{a_z^2 u}{4}\right] \\ & \times \left\langle \left[ \frac{1}{[(\sigma_y^2/\sigma_x^2 - 1)u + 1]} \frac{u}{[(1 - \sigma_x^2/\gamma^2\sigma_z^2)u + \sigma_x^2/\gamma^2\sigma_z^2]} \right]^{1/2} \right. \\ & \times I_0\left(\frac{a_y^2}{4} \frac{u}{(1 - \sigma_x^2/\sigma_y^2)u + \sigma_x^2/\sigma_y^2}\right) I_0\left(\frac{a_z^2 u}{4[(1 - \sigma_x^2/\gamma^2\sigma_z^2)u + \sigma_x^2/\gamma^2\sigma_z^2]}\right) \left. \right\rangle_s. \end{aligned} \quad (2.13)$$

From this general expression, we can obtain the tune shifts for special cases.

### A. Bunch length longer than the transverse sizes

Using the general expression Eq. (2.13) in this limit where the transverse sizes are both negligibly small compared to the bunch length, i.e.,  $(\sigma_x, \sigma_y) \ll \sigma_z$ , we find

$$\begin{aligned} \Delta\nu_x(a_x, a_y, a_z) = & C_{SC} \frac{R}{2\sqrt{2}\gamma\sigma_z\epsilon_x} \left\langle \int_0^1 du \exp\left[-\frac{a_z^2 u}{4}\right] I_0\left(\frac{a_z^2 u}{4}\right) \exp\left[-\frac{a_x^2 u}{4}\right] \left[ I_0\left(\frac{a_x^2 u}{4}\right) - I_1\left(\frac{a_x^2 u}{4}\right) \right] \right. \\ & \times \exp\left[-\frac{a_y^2 u}{4}\right] \left[ \frac{1}{[(\sigma_y^2/\sigma_x^2 - 1)u + 1]} \right]^{1/2} I_0\left(\frac{a_y^2}{4} \frac{u}{(1 - \sigma_x^2/\sigma_y^2)u + \sigma_x^2/\sigma_y^2}\right) \left. \right\rangle_s. \end{aligned} \quad (2.14)$$

Equation (2.14) and a similar one for  $\Delta\nu_y$  (with  $x \leftrightarrow y$ ) are of the form which is generally applicable for bunches in hadron synchrotrons, even the low energy machines where  $\gamma \simeq 1$ .

The tune shift at the origin is

$$\begin{aligned} \Delta\nu_{x,SC}(0,0,0) &= \frac{RC_{SC}}{2\sqrt{2}\gamma\epsilon_x\sigma_z} \int_0^1 du \left\langle \left[ \frac{1}{[(\sigma_y^2/\sigma_x^2 - 1)u + 1]} \right]^{1/2} \right\rangle_s \\ &= \frac{RC_{SC}}{\sqrt{2}\gamma\epsilon_x\sigma_z} \left\langle \frac{1}{1 + \sigma_y/\sigma_x} \right\rangle_s. \end{aligned} \quad (2.15)$$

Substituting the expression for  $C_{SC}$  and assuming round beams at all locations, we obtain

$$\begin{aligned} \Delta\nu_{x,SC} &= \frac{N_p r_p}{\beta^2 \gamma^2} \frac{R}{2\sqrt{2}\pi\gamma\sigma_z\epsilon_x} = \frac{r_p}{\beta\gamma^2\epsilon_{x,N}} \lambda_G R, \\ \lambda_G &= \frac{N_p}{2\sqrt{2}\pi\sigma_z}, \end{aligned} \quad (2.16)$$

where we used  $\epsilon_{x,N} = \beta\gamma\epsilon_x$  and  $\lambda_G$  is the longitudinal density. These are the standard expressions for the space charge tune shift parameters for Gaussian bunches. With a coasting bunch, the longitudinal density is  $\lambda = N_p/(2\pi R)$ .

The zero amplitude tune shifts for nonround beams can be written as

$$\begin{aligned} \Delta\nu_x(0,0,0) &= 2 \left\langle \frac{1}{\sigma_y/\sigma_x + 1} \right\rangle_s \Delta\nu_{x,SC}, \\ \Delta\nu_y(0,0,0) &= 2 \left\langle \frac{1}{\sigma_x/\sigma_y + 1} \right\rangle_s \Delta\nu_{y,SC}. \end{aligned} \quad (2.17)$$

These equations include the variation of beam sizes around the ring.

At zero transverse amplitude in this limit of both long and round bunches

$$\begin{aligned} \Delta\nu_x(0,0,a_z)|_{\text{Long,round}} &= \Delta\nu_{x,SC} \int_0^1 du \exp\left[-\frac{a_z^2 u}{4}\right] I_0\left(\frac{a_z^2 u}{4}\right) \equiv f_z \Delta\nu_{x,SC}, \end{aligned} \quad (2.18)$$

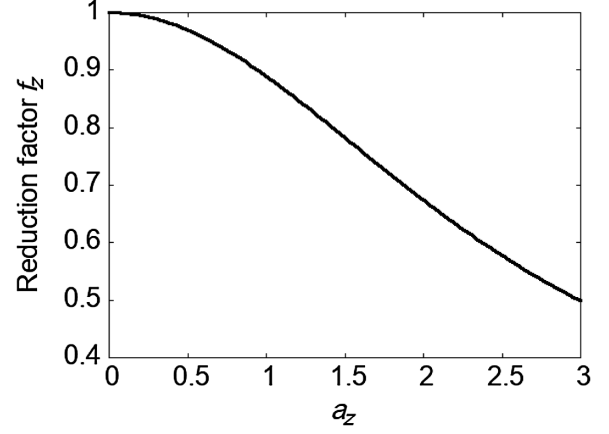


FIG. 1. Correction factor  $f_z$  for the reduction of the zero amplitude tune shift as a function of the longitudinal amplitude  $a_z$ .

$$f_z = \exp\left[-\frac{a_z^2}{4}\right] \left[ I_0\left(\frac{a_z^2}{4}\right) + I_1\left(\frac{a_z^2}{4}\right) \right], \quad (2.19)$$

where  $f_z$  is the correction factor that describes the impact of synchrotron oscillations. Hence  $f_z$  plotted in Fig. 1 shows that the small amplitude tune shifts due to the space charge of a longitudinal slice decreases with distance  $z$ , falling by half at  $a_z = 3$  corresponding to the edge of the bucket. The caveat is that the longitudinal motion is not simple harmonic; nevertheless, this curve should be accurate at smaller amplitudes. The small transverse amplitude particles can oscillate over different synchrotron amplitudes; we can average over the full range of these amplitudes. Assuming a Gaussian distribution in  $a_z$ , we find

$$\langle f_z \rangle = \frac{\sqrt{2}(\pi^2 - 2\Gamma[3/4]^4)}{\pi^{3/2}\Gamma[3/4]^2} \simeq 0.91. \quad (2.20)$$

We observe that synchrotron oscillation reduces the small amplitude tune shift by about 10%. However, since synchrotron oscillations have a much longer timescale than betatron oscillations, this average value  $\langle f_z \rangle$  may not be a useful indicator of their impact.

Zero synchrotron amplitude  $a_z = 0$  with arbitrary transverse sizes leads to

$$\begin{aligned} \Delta\nu_x(a_x, a_y, 0)|_{\text{Long}} &= \Delta\nu_{x,SC} \left\langle \int_0^1 du \exp\left[-\frac{a_x^2 u}{4}\right] \left[ I_0\left(\frac{a_x^2 u}{4}\right) - I_1\left(\frac{a_x^2 u}{4}\right) \right] \right. \\ &\quad \left. \times \exp\left[-\frac{a_y^2 u}{4}\right] \left[ \frac{1}{[(\sigma_y^2/\sigma_x^2 - 1)u + 1]} I_0\left(\frac{a_y^2}{4} \frac{u}{(1 - \sigma_x^2/\sigma_y^2)u + \sigma_x^2/\sigma_y^2}\right) \right] \right\rangle_s. \end{aligned} \quad (2.21)$$

We observe that when the beams are not round, the tune shift depends on the variation of the relative beam size  $\sigma_y/\sigma_x$  around the ring. The average over the ring can be calculated exactly with an integral evaluation at several points along the ring or approximately by replacing the average over the function by the function of the averaged

argument. This approach would require a single integral and would be computationally faster. The quality of this approximation will be evaluated in Sec. IV for IOTA parameters.

With the further assumption of round bunches everywhere, the above simplifies to

$$\begin{aligned} \Delta\nu_x(a_x, a_y, a_z)|_{\text{Long,round}} &= \Delta\nu_{x,\text{SC}} \int_0^1 du \exp\left[-\frac{a_z^2 u}{4}\right] I_0\left(\frac{a_z^2 u}{4}\right) \\ &\times \exp\left[-\frac{a_x^2 u}{4}\right] \left[ I_0\left(\frac{a_x^2 u}{4}\right) - I_1\left(\frac{a_x^2 u}{4}\right) \right] \exp\left[-\frac{a_y^2 u}{4}\right] I_0\left(\frac{a_y^2 u}{4}\right). \end{aligned} \quad (2.22)$$

In most machines, the bunch is not round everywhere in the ring; nevertheless, Eq. (2.22) can be used as a first approximation for the tune shift with amplitude.

In Sec. IV, we evaluate the tune shifts for IOTA parameters and consider the impact of synchrotron oscillations and the round beams approximation on the transverse tune shifts.

### B. Beam-beam tune shifts

The beam-beam tune footprint can be found in a similar fashion as given above. The major difference is that in a collider, the particles all move at very relativistic speed, so  $\beta \simeq 1$ ,  $\gamma \gg 1$ . Consequently, there is a large increase in the transverse fields in going from the rest frame to the lab frame due to the Lorentz boost while the longitudinal fields are unchanged,

$$\begin{aligned} \mathbf{E}_{\perp,\text{lab}} &\simeq \gamma \mathbf{E}_{\perp,\text{rest}} = -\gamma \nabla_{\perp} V_{\text{BB}}, & E_{z,\text{lab}} &= E_{z,\text{rest}}, \\ B_{x,\text{lab}} &= \frac{E_{y,\text{lab}}}{\beta}, & B_{y,\text{lab}} &= -\frac{E_{x,\text{lab}}}{\beta}. \end{aligned} \quad (2.23)$$

Here  $V_{\text{BB}}$  is the scalar potential for the beam-beam interaction and is the same as  $V_{\text{SC}}$  except that the beam parameters are of the opposing bunch. The net force due to the electric and magnetic fields is in the same direction for beam-beam interactions and oppose each other with space charge. While the space charge forces act radially outward in all directions, the beam-beam forces are almost entirely in the transverse plane emanating from a squashed pancake

like disc traveling with the opposing beam. In most circumstances, we can think of the opposing beam as being pointlike along the direction of motion and the beam-beam potential as effectively two dimensional. The longitudinal density has a role to play in beam-beam interactions in effects such as phase averaging in long bunches [11,12] or when hourglass effects [13] or crossing angles are introduced; see [14] for a recent calculation of the luminosity and beam-beam tune shifts with both these effects in a Higgs factory  $e^+ - e^-$  collider.

In most cases where the beam-beam interaction is 2D, the results of Sec. II A are applicable here because  $\gamma \gg 1$ . Following the same procedure as in obtaining Eq. (2.17) leads to the beam-beam tune shift at the origin

$$\begin{aligned} \Delta\nu_{x,bb} &= \frac{r_p N_p \beta_x^*}{2\pi\gamma} \frac{1}{\sigma_x^*(\sigma_x^* + \sigma_y^*)}, \\ \Delta\nu_{y,bb} &= \frac{r_p N_p \beta_y^*}{2\pi\gamma} \frac{1}{\sigma_y^*(\sigma_x^* + \sigma_y^*)}, \end{aligned} \quad (2.24)$$

where  $\beta_x^*, \beta_y^*, \sigma_x^*, \sigma_y^*$  are the values at the IP and we assumed that the beam parameters are the same at all the IPs.

The important point here is that both the space charge and the beam-beam potential have the same dependence on the transverse amplitudes, consequently, the two footprints are the same if we scale out the zero amplitude tune shifts. Thus, the horizontal beam-beam tune shift at transverse amplitudes  $(a_x, a_y)$  can be written down using Eq. (2.21)

$$\begin{aligned} \Delta\nu_{x,bb}(a_x, a_y) &= \Delta\nu_{x,bb} \int_0^1 du \exp\left[-\frac{a_x^2 u}{4}\right] \left[ I_0\left(\frac{a_x^2 u}{4}\right) - I_1\left(\frac{a_x^2 u}{4}\right) \right] \exp\left[-\frac{a_y^2 u}{4}\right] \\ &\times \left[ \frac{1}{[(\sigma_y^2/\sigma_x^2 - 1)u + 1]} I_0\left(\frac{a_y^2}{4} \frac{u}{(1 - \sigma_x^2/\sigma_y^2)u + \sigma_x^2/\sigma_y^2}\right) \right] \end{aligned} \quad (2.25)$$

and a similar expression holds in the vertical plane.

### III. DENSITY DISTRIBUTION IN TUNES

We saw in the previous section that the beam and machine parameters describing the space charge and beam-beam tune shifts are all included in the zero amplitude tune shifts  $\Delta\nu_{x,sc}$ ,  $\Delta\nu_{y,sc}$ . It is therefore useful to describe the universal functions of the dimensionless amplitudes as

$$\begin{aligned}\xi_x(a_x, a_y, a_z) &= \frac{\Delta\nu_x(a_x, a_y, a_z)}{\Delta\nu_{x,sc}}, \\ \xi_y(a_x, a_y, a_z) &= \frac{\Delta\nu_y(a_x, a_y, a_z)}{\Delta\nu_{y,sc}}.\end{aligned}\quad (3.1)$$

The functions  $\xi_x$ ,  $\xi_y$  are universal in the sense that their behavior describes the amplitude dependence for any machine. In this section, we consider the distribution assuming a Gaussian distribution in phase space.

#### A. Density distribution in 1D

We start with the tune density distribution in 1D for the sake of clarity. The density in action  $j_x$  is transformed to the dimensionless amplitude variable  $\alpha_x$  as

$$\rho(j_x) = \frac{1}{\varepsilon_x} \exp\left[-\frac{j_x}{\varepsilon_x}\right] = \frac{1}{\varepsilon_x} \exp[-2\alpha_x], \quad \alpha_x = \frac{a_x^2}{4} = \frac{j_x}{2\varepsilon_x}, \quad (3.2)$$

$$\begin{aligned}\rho(\alpha_x) &= \rho(a_x) \left[\frac{\partial\alpha_x}{\partial a_x}\right]^{-1} = a_x \exp\left[-\frac{1}{2}a_x^2\right] [a_x/2]^{-1} \\ &= 2 \exp[-2\alpha_x].\end{aligned}\quad (3.3)$$

Now we need to transform from the amplitude to the scaled tune shift which implies

$$\begin{aligned}\rho(\xi_x) &= \frac{\rho(\alpha_x)}{d\xi_x/d\alpha_x} = \frac{1}{2} \exp[-2\alpha_x] \\ &\times \left[ \int_0^1 du u [H'_0(\alpha_x u) - H'_1(\alpha_x u)] \right]^{-1},\end{aligned}\quad (3.4)$$

$$H_n(z) \equiv \exp[-z] I_n(z). \quad (3.5)$$

Hence, using the tune shift expression in 1D

$$\xi_x(\alpha_x) = \int_0^1 du [H_0(\alpha_x u) - H_1(\alpha_x u)], \quad (3.6)$$

$$\begin{aligned}\rho(\xi_x) &= \rho(\alpha_x) \left[\frac{\partial\xi_x}{\partial\alpha_x}\right]^{-1} \\ &= 2 \exp[-2\alpha_x] \left[ \int_0^1 du u [H'_0(\alpha_x u) - H'_1(\alpha_x u)] \right]^{-1}\end{aligned}\quad (3.7)$$

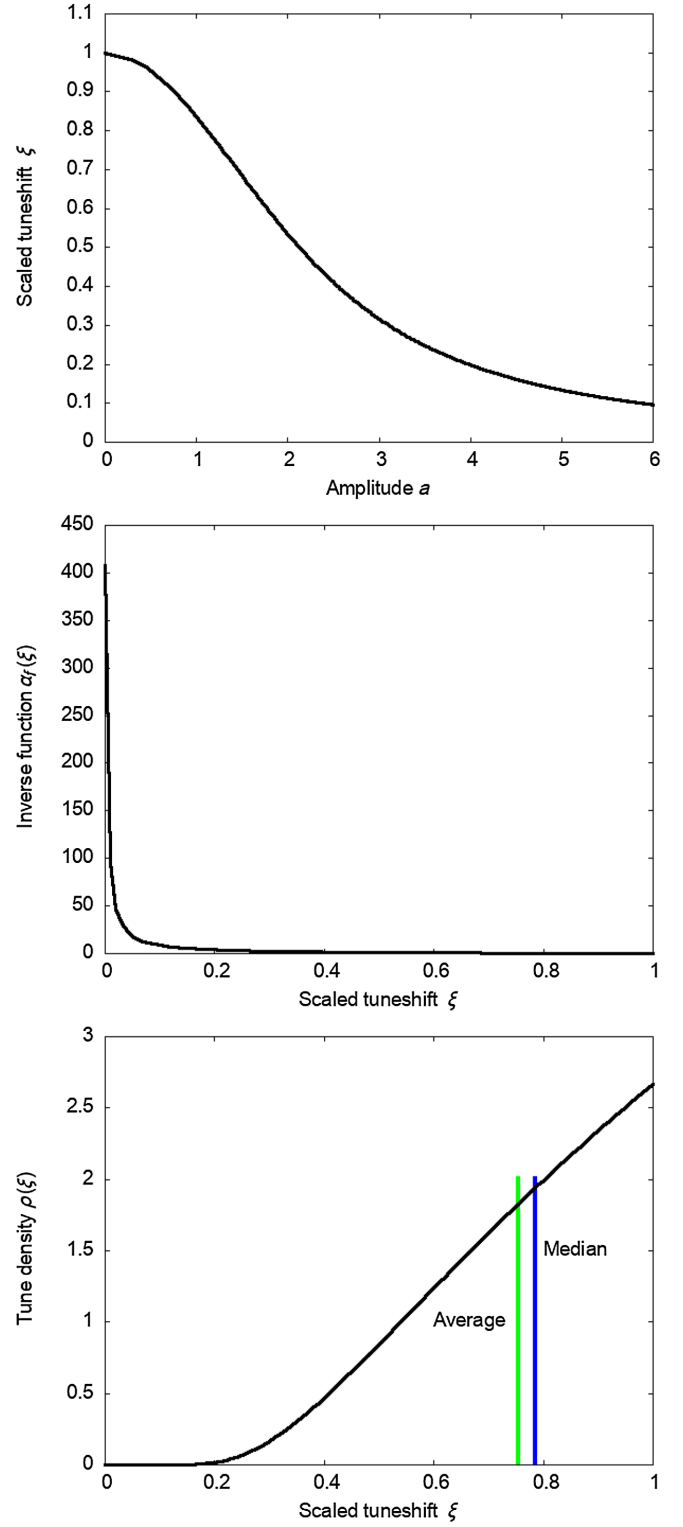


FIG. 2. Top: Tune shift  $\xi$  as a function of the scaled amplitude  $a_x = 2\sqrt{\alpha_x}$ ,  $a_x$  is the transverse amplitude in units of the rms size; Middle: the inverse function  $\alpha_x(\xi)$ . Bottom: the density distribution as a function of the tune shift.



$$\equiv 2 \frac{\exp[-2\alpha_x]}{\text{Jac}(\alpha_x, \xi_x)}. \quad (3.8)$$

Here  $\text{Jac}(\alpha_x, \xi_x)$  is the Jacobian of the transformation from  $\alpha_x \rightarrow \xi_x$ . Equation (3.6) defines  $\xi_x$  as a function of  $\alpha_x$ . Inverting this relation (numerically) defines  $\alpha_x$  as a function of  $\xi_x$ . We denote this function  $\alpha_f(\xi_x)$ . Inserting this function back into Eq. (3.8) yields the functional form

$$\rho(\xi_x) = 2 \frac{\exp[-2\alpha_f(\xi_x)]}{\text{Jac}[\alpha_f(\xi_x)]}. \quad (3.9)$$

In 1D, the inverse function is straightforward to obtain. Figure 2 shows plots of the function  $\xi_x(\alpha_x)$  and the inverse

$$\begin{aligned} \langle \xi_x \rangle &= \int_0^\infty \xi(\alpha_x) \rho(\alpha_x) d\alpha_x = 2 \int_0^\infty \exp[-2\alpha_x] d\alpha_x \int_0^1 du [H_0(\alpha_x u) - H_1(\alpha_x u)] \\ &= 2 \int_0^\infty d\alpha_x \int_0^1 du \exp[-(2+u)\alpha_x] [I_0(\alpha_x u) - I_1(\alpha_x u)]. \end{aligned} \quad (3.11)$$

We use the integration result from the table of integrals in [15]

$$\int_0^\infty e^{-\alpha z} I_p(\beta z) dz = \frac{\beta^p}{\sqrt{\alpha^2 - \beta^2} (\alpha + \sqrt{\alpha^2 - \beta^2})^p}. \quad (3.12)$$

Doing the integral over  $\alpha_x$  first followed by the integration over  $u$ , we find

$$\begin{aligned} \langle \xi_x \rangle &= \int_0^\infty d\alpha_x \exp[-(2+u)\alpha_x] [I_0(\alpha_x u) - I_1(\alpha_x u)] \\ &= \int_0^1 du \left[ \frac{1}{\sqrt{1+u}} - \frac{1}{\sqrt{1+u}} \frac{u}{(1+\sqrt{1+u})^2} \right] \end{aligned} \quad (3.13)$$

$$= 4(\text{arcsinh}[1] - \log[2]) = 0.752906. \quad (3.14)$$

Numerically, the moments can also be calculated using either  $\rho(\alpha_x)$  or  $\rho(\xi_x)$ . The results are shown in Table I where numerical A uses the first method and numerical B uses the second. The fact that the moments calculated numerically with numerical B agrees exactly with the other methods gives confidence that the expression for the density distribution in tune shift  $\rho(\xi_x)$  is correct.

Finally, we calculate the median tune shift which by definition is the value at which the number of particles is the same both above and below the median value  $\xi_m$ , i.e.,

$$\int_0^{\xi_m} \rho(\xi_x) d\xi_x = \int_{\xi_m}^\infty \rho(\xi_x) d\xi_x = 0.5 \rightarrow \xi_m = 0.783. \quad (3.15)$$

The density distribution  $\rho(\xi_x)$  along with the average and median tune shifts are indicated in the bottom plot of Fig. 2.

function  $\alpha_f(\xi_x)$  which resembles a one-sided delta function.

The  $p$ th moment of the tune shift, i.e.,  $\langle \xi_x^0 \rangle$  (the norm),  $\langle \xi_x^1 \rangle$ ,  $\langle \xi_x^2 \rangle$ , ... should agree in any coordinate system used for the density distribution. We can use this to test the accuracy of the distribution in  $\xi_x$ . The two lowest moments can be calculated analytically using the known functional forms in terms of  $\alpha_x$ .

$$\int_0^1 \rho(\xi_x) d\xi_x = \int_0^\infty \rho(\alpha_x) d\alpha_x = 2 \int_0^\infty \exp[-2\alpha_x] d\alpha_x = 1, \quad (3.10)$$

The 1D density vanishes in the range  $a \leq \xi_x \leq 0.2$  and reaches a maximum at  $\xi_x = 1$ , as expected since that is the region of maximum density.

## B. Density distribution in 2D

The procedure is the same as in 1D, but the details are slightly different because first a nonlinear equation in two variables has to be solved followed by a 2D interpolation is required. Let the density in the tune space be  $\rho(\xi_x, \xi_y)$ . By the conservation of particle number,

$$\rho(\alpha_x, \alpha_y) d\alpha_x d\alpha_y = \rho(\xi_x, \xi_y) d\xi_x d\xi_y, \quad (3.16)$$

which implies

TABLE I. Moments of the density distribution calculated in different ways in 1D and 2D. The two numerical ways, labeled as i and ii, describe using the density in amplitude space  $\rho(\alpha_x, \alpha_y)$  and tune space  $\rho(\xi_x, \xi_y)$ , respectively. In all cases, numerical A is the more accurate.

	Analytical	Numerical A	Numerical B
	1D		
Normalization	1.0	1.0	1.0
$\langle \xi_x \rangle$	0.752906	0.752906	0.752906
$\langle \xi_x^2 \rangle$	Not applicable	0.597766	0.597766
$\xi_{x,\text{rms}}$	Not applicable	0.175782	0.175782
	2D		
Normalization	1.0	1.0	0.981
$\langle \xi_x \rangle$	0.633389	0.633389	0.629
$\langle \xi_x^2 \rangle$	Not applicable	0.4293	0.4596
$\xi_{x,\text{rms}}$	Not applicable	0.1678	0.253

$$\rho(\xi_x, \xi_y) = \rho(\alpha_x, \alpha_y) / \text{Jac}(\xi_x, \xi_y; \alpha_x, \alpha_y), \quad (3.17)$$

where

$$\text{Jac}(\xi_x, \xi_y; \alpha_x, \alpha_y) = \left\| \begin{array}{cc} \frac{\partial \xi_x}{\partial \alpha_x} & \frac{\partial \xi_x}{\partial \alpha_y} \\ \frac{\partial \xi_y}{\partial \alpha_x} & \frac{\partial \xi_y}{\partial \alpha_y} \end{array} \right\|. \quad (3.18)$$

The density can be written as

$$\rho(\alpha_x, \alpha_y) = 4 \exp[-2\alpha_x - 2\alpha_y]. \quad (3.19)$$

In terms of these variables, the scaled tune shifts are

$$\xi_x(\alpha_x, \alpha_y) = \int_0^1 du [H_0(\alpha_x u) - H_1(\alpha_x u)] H_0(\alpha_y u), \quad (3.20)$$

$$\xi_y(\alpha_x, \alpha_y) = \int_0^1 du H_0(\alpha_x u) [H_0(\alpha_y u) - H_1(\alpha_y u)]. \quad (3.21)$$

The derivatives are found for example as

$$\frac{\partial \xi_x}{\partial \alpha_x} = \left( \int_0^1 du u H_0(\alpha_x u) [H'_0(\alpha_x u) - H'_1(\alpha_x u)] H_0(\alpha_y u) \right). \quad (3.22)$$

These can be used to write the density in tune space using Eqs. (3.17)–(3.19) in terms of  $\alpha_x, \alpha_y$ . Doing so yields

$$\rho(\xi_x, \xi_y) = 4 \frac{\exp[-2\alpha_x - 2\alpha_y]}{\text{Jac}(\xi_x, \xi_y; \alpha_x, \alpha_y)}. \quad (3.23)$$

The rhs of this equation, however, is a function of the amplitudes  $(\alpha_x, \alpha_y)$  while what we want is a function of the scaled tune shifts  $(\xi_x, \xi_y)$ . That requires an inversion of Eqs. (3.20) and (3.21). It is done in two steps: (i) solving these nonlinear equations to find  $\alpha_x, \alpha_y$  as functions of  $\xi_x, \xi_y$  and (ii) interpolating these as smooth functions of  $\xi_x, \xi_y$ . Figure 3 shows the complete density  $\rho(\xi_x, \xi_y)$  as a function of  $\xi_x, \xi_y$  viewed from two different angles as well the projected density  $\rho_x(\xi_x)$  on the  $\xi_x$  axis, which is obtained by integrating over the  $\xi_y$  axis, i.e.,

$$\rho_x(\xi_x) = \int_0^1 d\xi_y \rho(\xi_x, \xi_y). \quad (3.24)$$

The density is exactly symmetric along the  $\xi_x = \xi_y$  axis, as it must be for round beams. The second plot shows that the density is zero at the origin and we observe that along either the  $\xi_x$  axis or the  $\xi_y$  axis, the density is similar to the 1D density profile seen in Fig. 2. The projected density does not vanish at  $\xi_x = 0$  and it has a maximum around  $\xi_x = 0.9$  rather than at  $\xi_x = 1$ . A little thought shows that is

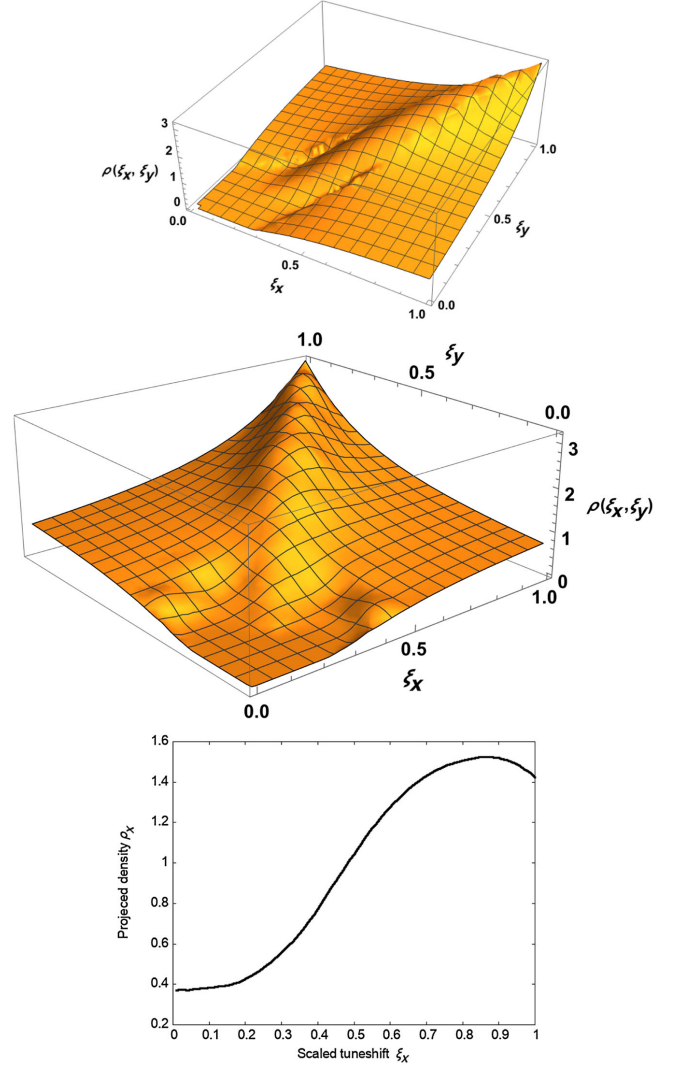


FIG. 3. Top: density  $\rho(\xi_x, \xi_y)$  vs the scaled tune shifts  $\xi_x, \xi_y$ . Middle: this plot shows the density from a different angle, it shows, e.g., the density along the  $\xi_x$  and also along the  $\xi_y$  axes. Bottom: the projected density  $\rho_x$  along the  $\xi_x$  axis. It is nonzero at  $\xi_x = 0$  and it has a maximum at a value less than  $\xi_x = 1$ .

true of any density that has a nonvanishing dependence on both  $\alpha_x, \alpha_y$ .

The moments of the distribution are found as before

$$\begin{aligned} \langle \xi_x \rangle &= \int_0^\infty d\alpha_x \int_0^\infty d\alpha_y \xi_x(\alpha_x, \alpha_y) \rho(\alpha_x, \alpha_y) \\ &= 4 \int_0^1 du \int_0^\infty d\alpha_x \int_0^\infty d\alpha_y [H_0(\alpha_x u) - H_1(\alpha_x u)] \\ &\quad \times H_0(\alpha_y u) \exp[-2\alpha_x - 2\alpha_y]. \end{aligned} \quad (3.25)$$

For the integration over  $\alpha_y$ , we use the same integral result in Eq. (3.12) to obtain



$$\int_0^\infty H_0(\alpha_y u) \exp[-2\alpha_x - 2\alpha_y] d\alpha_y = \frac{1}{\sqrt{1+u}}.$$

Combining this integration and doing the final integral over  $u$ , we find

$$\langle \xi_x \rangle = 4 \ln \left[ \frac{2\sqrt{2}}{\sqrt{2}+1} \right] = 0.633389. \quad (3.26)$$

The moments calculated numerically using both methods used for the 1D distribution are shown in Table I. The normalization is not quite unity with the second method. We attribute this  $\sim 2\%$  error to numerical issues in the inversion and interpolation required to find the functions  $\alpha_x(\xi_x, \xi_y)$ ,  $\alpha_y(\xi_x, \xi_y)$ . This can be used to find the correct moments by dividing the raw moments by the normalization. With this correction, the error in the first moment is  $\sim 0.7\%$  while the error in the second moment is  $7\%$ .

We briefly consider the application of these results to beam stability with octupoles and space charge, a more detailed study will be reported elsewhere. Typically, the stability is considered using the dispersion relation with a 2D betatron spread from both octupoles and space charge. This relation was used to derive stability curves [16] with a parabolic transverse density which results in a space charge tune spread linear in the actions that matches the octupolar tune spread dependence. It may be possible to use the exact space charge tune spread  $\Delta\nu_{x,SC}(a_x, a_y) = \Delta\nu_{x,SC}\xi_z(a_x, a_y)$  to obtain stability curves for Gaussian bunches. The extension to 3D stability is in principle straightforward, using the 3D space charge tune shifts  $\xi_{x,y}(a_x, a_y, a_z)$  found in Sec. II. A more direct use of the density curves derived in this section would be to check the results derived from PIC simulations against the exact results obtained here. We also note that the rms tune spread calculated in Table I may be directly related to the decoherence time following a kick; this time in 2D is longer than the typical  $1/\Delta\nu_{SC}$  timescale associated with 1D decoherence.

#### IV. APPLICATION TO IOTA

IOTA is an accelerator that was designed to test the concept of nonlinear integrable lattices [17]. The R & D program with electrons and protons was discussed in [18]. The ring has been operated with electrons since commissioning began and several notable results have been achieved, including the demonstration of optical stochastic cooling [19]. Proton operation is scheduled to begin in 2024 when the concept of achieving high space charge tune shifts with a nonlinear integrable lattice will be tested.

In this section, we will evaluate the space charge footprints theoretically and compare them with particle tracking. This is done in an otherwise completely linear lattice; we note that emittance growth and beam loss were studied in a partially integrable lattice with octupoles in [20]. Table II shows the relevant parameters of the IOTA

TABLE II. Machine and beam parameters of the IOTA proton ring.

IOTA proton parameters	
Circumference	39.97 (m)
Kinetic energy	2.5 (MeV)
Maximum bunch intensity/current	$9 \times 10^{10}/8$ (ma)
Transverse normalized rms emittance	(0.3, 0.3) (mm mrad)
Betatron tunes	(5.3, 5.3)
Natural chromaticities	(-8.2, -8.1)
Average transverse beam sizes (rms)	(2.22, 2.22) (mm)
Kinematic $\gamma$ /transition $\gamma_t$	1.003/3.75
rf voltage	400 (volts)
rf frequency/harmonic number	2.2 (MHz)/4
Bucket length	$\sim 10$ (m)
Bucket half height in $\delta p/p$	$3.72 \times 10^{-3}$
rms bunch length	1.7 (m)
rms energy/momentum spread	$1.05 \times 10^{-5}/1.99 \times 10^{-3}$
Synchrotron tune/period [turns]	0.0069/ $\sim 145$

proton ring. First, we consider whether the beam is sufficiently round everywhere in the ring for the round beam expressions for the footprint to be applicable. Figure 4 shows the ratio of the vertical to horizontal beam sizes along the ring. The ratio varies between 0.5 and 5.0 with a mean value of 1.2. The mean value may not be relevant here, as the fluctuations are fairly large. We therefore use the general expression for the tune shifts but we also compare with the round beam forms as well as an approximation discussed in Sec. II. We discuss first the theoretical footprints under the different assumptions discussed in Sec. II. In the limit of long bunches, which is valid for IOTA, we can use Eq. (2.13). This involves calculating the tune shift at each longitudinal location and averaging over the locations. This method requires doing an integration at each location. We can reverse the order and instead do the averaging first and do a single integration instead.

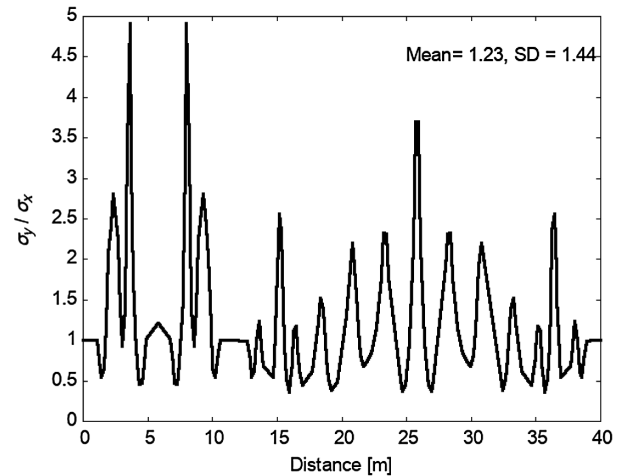


FIG. 4. Ratio of  $\sigma_y/\sigma_x$  around the ring.

$$\Delta\nu_x(a_x, a_y, a_z) = \Delta\nu_{x,SC} \int_0^1 du \left\{ \left\langle \exp\left[-\frac{a_z^2 u}{4}\right] I_0\left(\frac{a_z^2 u}{4}\right) \exp\left[-\frac{a_x^2 u}{4}\right] \left[ I_0\left(\frac{a_x^2 u}{4}\right) - I_1\left(\frac{a_x^2 u}{4}\right) \right] \right. \right. \\ \left. \left. \times \exp\left[-\frac{a_y^2 u}{4}\right] \left[ \frac{1}{[(\sigma_y^2/\sigma_x^2 - 1)u + 1]} \right]^{1/2} I_0\left(\frac{a_y^2 u}{4} \frac{u}{(1 - \sigma_x^2/\sigma_y^2)u + \sigma_x^2/\sigma_y^2}\right) \right\rangle_s \right\}. \quad (4.1)$$

This reduces the time required for evaluation and we found that the differences in numerical values are negligible, at least in the case of IOTA.

The left plot in Fig. 5 shows a comparison of the footprints based on the general expression in Eq. (2.13) and that based on the round beam expression in Eq. (2.22). The differences are small; this is, to be expected as IOTA has been designed to have axial symmetry almost everywhere in the ring in order to preserve integrability [17]. The right plot in this figure shows the footprints with synchrotron oscillations at two amplitudes  $a_z = 1, 2$ . As expected in Fig. 1, the total tune shift at  $a_z = 1$  is about 90% and at  $a_z = 2$ , the total tune shift is 70% of the value at  $a_z = 0$ .

The theory of the amplitude dependent tune shifts assumes that the particles stay at constant amplitudes while executing betatron oscillations. This is not always true, especially at high intensities. We examine this assumption by testing emittance growth with PyOrbit simulations [21]. Many details on the PyOrbit simulations and their validation can be found in earlier reports [20,22]. Detailed analysis had shown that there was good agreement between theory and simulations in all the tested regimes. In the simulations reported here, all machine nonlinearities were turned off, space charge was the only nonlinearity. The results reported in [22] showed that initial beam losses can be minimized by a process of slow initialization in which the charge per macroparticle is increased over about 100 turns to full value and the beam was injected into a lattice that was rms matched to equilibrium beam sizes. The PIC parameters that led to convergence were found to have the following values: number of macroparticles =  $5 \times 10^5$ , grid size

=  $128 \times 128 \times 5$ , and the number of space charge kicks per betatron wavelength = 63. These values were used in the simulations discussed below.

It is not completely straightforward to compare space charge simulations with theory, especially at high intensities. The simplest is to compare the space charge tune shifts. The complications arise from the two effects theory which assumes that the tune shift is calculated at constant emittances, which is not the case as the space charge increases. The second complication is related to PIC simulations. It has been observed that this method causes orbits to be chaotic at small amplitudes close to the origin [23]. We dealt with the first issue by using the average emittance over the time used for the tuneshift calculation. For the second issue, we distribute particles over 100 different angles at the same small amplitude and average over the angles to reduce the fluctuations in the tune shift value. Another complication at high intensities is that because the FFT aliases tunes to be in the range 0–0.5, it cannot determine if the tunes are below or above the half integer when the space charge tune shift exceeds 0.5. Here we determined the correct tune shifts by selecting the value that increased with intensity, without deeming the integer parts. Previously, we had determined the complete tune (integer and fractional parts) with the alternative method of counting the number of betatron oscillations over a thousand turns and found that the simulated tunes calculated both ways agreed well with each other and with theory [22].

At a low intensity of  $10^9$  particles/bunch, there are only fluctuations due to numerical noise in the PIC simulations. These are observed to be around 0.4%, which is close to the

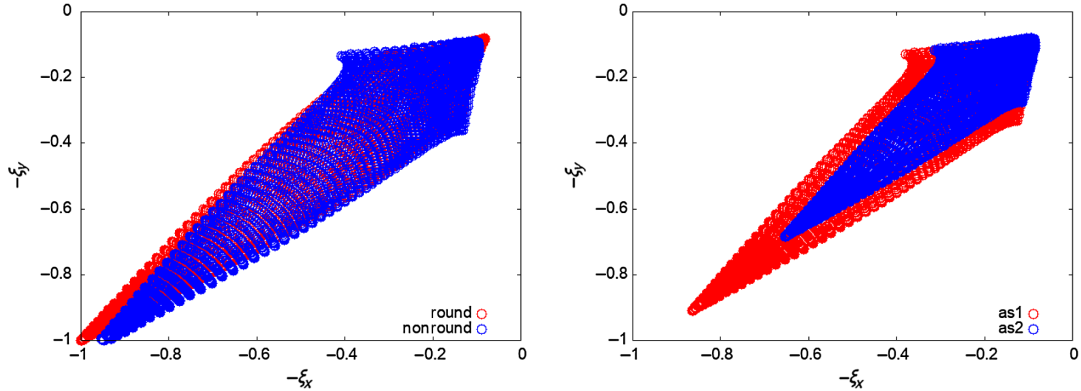


FIG. 5. Left: comparison of round and nonround footprints without synchrotron oscillations. Right: footprints with synchrotron oscillation amplitudes of  $1\sigma_s$  (in red) and  $2\sigma_s$  (blue).

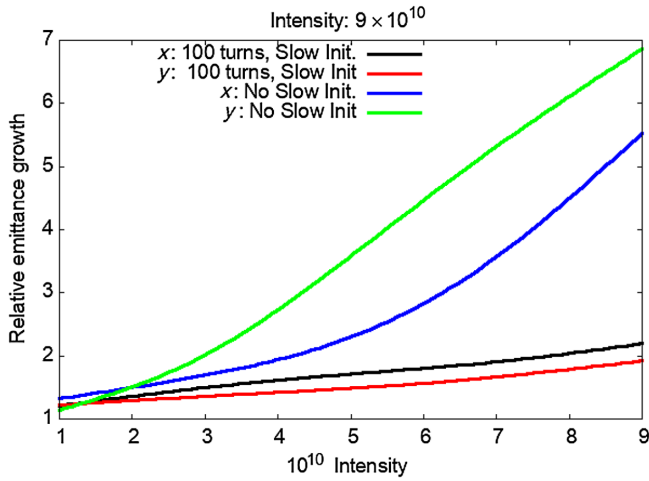


FIG. 6. Relative emittance growth over 1000 turns as a function of the intensity for two conditions: without slow initialization and with a slow initialization of 100 turns.

expected level  $\sim 1/\sqrt{n} = 0.14\%$  with  $n = 5 \times 10^5$ . Figure 6 shows the emittance change over a range of intensities; the last value  $9 \times 10^{10}$  corresponds to the maximum design bunch intensity. Since there is very little observable

emittance growth at the lowest intensities in this range, we expect the simulated tunes to be close to theoretical values. However, the tune shifts are too small to be accurately computable with an FFT over  $\sim 1000$  turns, especially to resolve the tune shift for neighboring particles. We use a Hann filter to improve the FFT resolution. At intermediate intensity of  $10^{10}$ , there is a larger emittance growth of  $\sim 10\%$  while at  $9 \times 10^{10}$ , the emittance grows by nearly a factor of 10 without slow initialization. The tune footprints are calculated using  $5 \times 10^5$  macroparticles and using 5000 test particles distributed transversely from 0 to  $5\sigma$  and with zero synchrotron amplitude. Figure 7 shows the footprints at  $10^{10}$  and  $9 \times 10^{10}$  intensities obtained with PyOrbit simulations and compared with the theoretical values using Eq. (2.21). In the top plots of Fig. 7, we have scaled the numerical footprints by the maximum tune shift, so the analytical and numerical footprints can be easily compared. In the bottom plots of this figure, we show the absolute footprints are shown except at the higher intensity, the fractional parts are shown since these are the FFT values. At the lower intensity, the two footprints agree reasonably well although the simulated footprint is wider at amplitudes from 1 to  $5\sigma$ . At the intensity of  $9 \times 10^{10}$ , the simulated

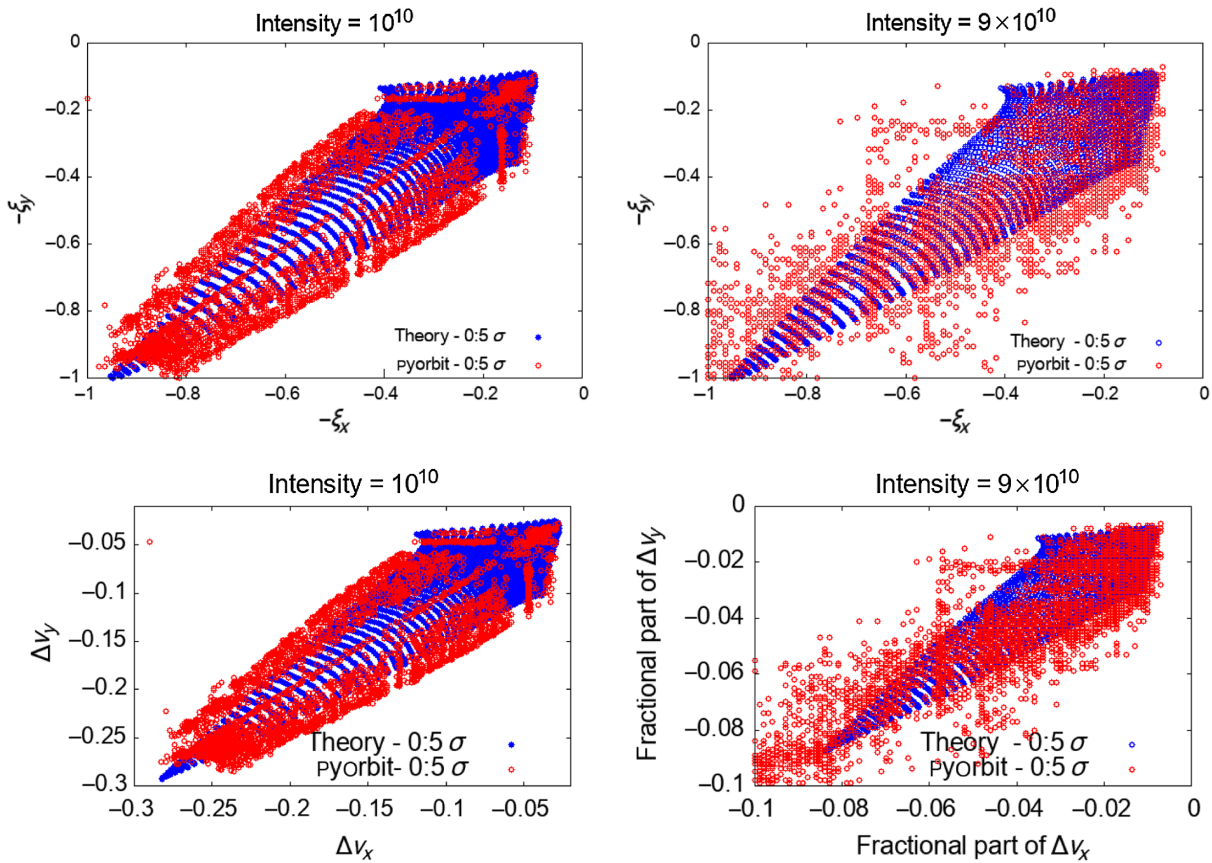


FIG. 7. Top row: scaled footprints from pyorbit tracking and theory with nonround beams with  $a_z = 0$ . Left: intensity =  $10^{10}$ , Right: intensity =  $9 \times 10^{10}$ . Bottom row: absolute footprints at the same intensities as above. At the higher intensity, the footprint shows the fractional part only, the total tune shifts are an integer higher at  $(-1 + [\Delta\nu_x], -1 + [\Delta\nu_y])$ , and the  $[\ ]$  denotes the fractional part.

footprint is even wider and the agreement is not as close, which is to be expected. The single most important reason for the increasing discrepancy is that the theory assumes that all particles move on invariant actions which is not true at high intensities. Nevertheless, the theoretical footprint can be useful both as a benchmark tool and also to quickly determine the important resonances that can be crossed by the footprint at a chosen working point.

## V. CONCLUSIONS

We derived tune shifts with amplitude in terms of a universal dimensionless parameter under quite general conditions that are valid for space charge or beam-beam interactions. We included multiple interaction points and synchrotron oscillations. Our focus is on space charge interactions mainly and the inclusion of multiple interactions as well as beams with arbitrary transverse aspect ratios is especially important. We then used the analytical tune shifts to derive semianalytical expressions for the density distribution of tunes assuming that the density is a Gaussian function of the phase-space coordinates. The tune distribution requires an inversion of the functional arguments followed by a numerical interpolation. We emphasize that the tune distribution thus obtained requires no numerical simulations. This is important because the density at the maximum tune shift requires very high sampling of this region and quite often the simulations get the wrong shape of the density in this region. The density is expressed in terms of variables  $(\xi_x, \xi_y)$  which are the tune shifts scaled by the maximum tune shifts. Therefore, the density  $\rho(\xi_x, \xi_y)$  has the same form and shape for both space charge and beam-beam interactions. With the method presented here, we verified that the low order moments of the distribution are preserved in the transformation; exactly in 1D and with a  $\sim 2\%$  error in 2D for the zeroth moment, see Table I for the other moments. These errors could be further reduced by improving the numerical schemes for the function inversion and interpolation. This calculation of the density distribution in tunes will enable a more accurate modeling of Landau damping with space charge and an external nonlinearity such as octupoles as well as the damping with beam-beam interactions.

We checked the tune spread calculations for the IOTA proton ring with simulations using the PyOrbit code. At the highest intensities planned with bunched beams, there is a substantial emittance blow up and steps will need to be taken to mitigate emittance growth and beam loss. We used a numerical scheme of slow initialization to reduce the growth and prevent beam loss over the short timescale of the simulation. Using this scheme, we found generally good agreement between the footprints calculated by theory and simulation. The expressions for the theoretical footprints developed in this paper should therefore be useful for benchmarking other space charge simulation codes as well as determining working points relatively free of low order space charge driven resonances.

## ACKNOWLEDGMENTS

I thank former undergraduate interns David Feigelson (University of Chicago) and Runze Li (UW, Madison; now at Yale) and colleague Francois Ostiguy for their enthusiastic collaboration on a project to model space charge effects in IOTA. I am especially thankful to Runze for writing a library of PyOrbit codes needed for modeling IOTA; these codes are available at his github site [24]. The work has been supported by the Fermi Research Alliance, LLC under Contract No. DE-AC02-07CH11359 with the U.S. Department of Energy, Office of Science, Office of High Energy Physics.

- 
- [1] X. Buffat, W. Herr, N. Mounet, T. Pieloni, and S. White, Stability diagrams of colliding beams in the Large Hadron Collider, *Phys. Rev. ST Accel. Beams* **17**, 111002 (2014).
  - [2] D. Mohl, Landau damping of dipole modes by space charge and octupoles, CERN Report No. CERN/PS-95-08 (DI).
  - [3] V. Shiltsev, Y. Alexahin, A. Burov, and A. Valishev, Landau Damping of Beam Instabilities by Electron Lenses, *Phys. Rev. Lett.* **119**, 134802 (2017).
  - [4] A. W. Chao, Beam-beam instability, SLAC Report No. SLAC-PUB-3179, 1983.
  - [5] A. W. Chao, P. Bambade, and W. T. Weng, Nonlinear beam-beam resonances, SLAC Report No. SLAC-PUB-3545, 1985.
  - [6] E. Keil, Beam-beam dynamics, CERN Report No. CERN-SL-94-78-AP, 1994.
  - [7] T. Sen, Head-on beam-beam interactions in the Tevatron (unpublished notes), ca. 2003.
  - [8] T. Sen, B. Erdelyi, M. Xiao, and V. Boochoa, Beam-beam effects at the Fermilab Tevatron: Theory, *Phys. Rev. ST Accel. Beams* **7**, 041001 (2004).
  - [9] K. Y. Ng, Distribution of incoherent space charge tune shift for a bi-Gaussian beam, FERMILAB Report No. TM-2241, 2004.
  - [10] K. Takayama, A new method for the potential of a 3 dimensional nonuniform charge distribution, *Lett. Nuovo Cimento* **34**, 190 (1982).
  - [11] S. Krishnagopal and R. Siemann, Bunch length effects in the beam-beam interaction, *Phys. Rev. D* **41**, 2312 (1990).
  - [12] T. Sen, The beam-beam interaction of finite length bunches in hadron colliders, FNAL Report No. FNAL-Pub-00/093-T, 2000.
  - [13] M. Furman, The hourglass reduction factor for asymmetric colliders, SLAC Report No. SLAC-ABC-21A, 1991.
  - [14] T. Sen, Luminosity and beam-beam tune shifts with crossing angle and hourglass effects in an  $e^+ e^-$  colliders, [arXiv:2208.08615](https://arxiv.org/abs/2208.08615).
  - [15] I. S. Gradshteyn and I. M. Ryzhik, *Table of Integrals, Series and Products* (Academic Press, New York, 1980).
  - [16] E. Metral and F. Ruggiero, Stability diagrams for Landau damping with two-dimensional betatron tune spread from both octupoles and nonlinear space charge applied to the LHC at injection, CERN Report No. CERN-AB-2004-067.



- [17] V. Danilov and S. Nagaitsev, Nonlinear accelerator lattices with one and two analytic invariants, *Phys. Rev. ST Accel. Beams* **13**, 084002 (2010).
- [18] S. Antipov *et al.*, IOTA (Integrable Optics Test Accelerator): Facility and experimental beam physics program, *J. Instrum.* **12**, T03002 (2017).
- [19] J. Jarvis *et al.*, Experimental demonstration of optical stochastic cooling, *Nature (London)* **608**, 287 (2022).
- [20] D. Feigelson, T. Sen, J.-F. Ostiguy, and R. Li, Space charge driven emittance growth and the effect of octupoles in IOTA, [arXiv:2112.15306](https://arxiv.org/abs/2112.15306).
- [21] <https://github.com/PyORBIT-Collaboration/py-orbit>.
- [22] R. Li, T. Sen, and J.-F. Ostiguy, Modeling Transverse Space Charge effects in IOTA with pyORBIT, Fermilab Report No. FERMILAB-TM-2753-AD.
- [23] F. Schmidt *et al.*, Code bench-marking for long-term tracking and adaptive algorithms, in *Proceedings of the 57th ICFA Advanced Beam Dynamics Workshop on High-Intensity, High Brightness and High Power Hadron Beams, HB2016, Malmö, Sweden* (2016), p. 357
- [24] [https://github.com/Patchouligoo/pyorbit\\_iota](https://github.com/Patchouligoo/pyorbit_iota).